Active random forces can drive differential cellular positioning and enhance motor-driven transport

Charles W. Wolgemuth[a,b,*] and Sean X. Sun[a,c]
[a]Johns Hopkins Physical Sciences–Oncology Center and [c]Department of Mechanical Engineering, Johns Hopkins University, Baltimore, MD 21218; [b]Departments of Physics and Molecular and Cellular Biology, University of Arizona, Tucson, AZ 85721

ABSTRACT **Cells are remarkable machines capable of performing an exquisite range of functions, many of which depend crucially on the activity of molecular motors that generate forces. Recent experiments have shown that intracellular random movements are not solely thermal in nature but also arise from stochasticity in the forces from these molecular motors. Here we consider the effects of these nonthermal random forces. We show that stochastic motor force not only enhances diffusion but also leads to size-dependent transport of objects that depends on the local density of the cytoskeletal filaments on which motors operate. As a consequence, we find that objects that are larger than the mesh size of the cytoskeleton should be attracted to regions of high cytoskeletal density, while objects that are smaller than the mesh size will preferentially avoid these regions. These results suggest a mechanism for size-based organelle positioning and also suggest that motor-driven random forces can additionally enhance motor-driven transport.**

Monitoring Editor
Alex Mogilner
New York University

Received: Nov 15, 2019
Revised: Jun 17, 2020
Accepted: Jul 21, 2020

INTRODUCTION

Inside cells, molecular motors use chemical reactions to ratchet favorable thermal fluctuations in order to generate the forces that power many cellular processes, such as organelle transport, cell division, and motility (Oster, 2002; Kolomeisky and Fisher, 2007). However, because the cytoskeleton that motors operate on are disordered and the chemical reactions are stochastic, active forces that these motors create are themselves random in magnitude and orientation. Recent experiments have quantified the intracellular random motions generated by the forces from molecular motors and have shown that these random motions are nonequilibrium in nature (Martin *et al.*, 2001; Guo *et al.*, 2014); that is, they are not constrained by the physics governing equilibrium conditions, such as the fluctuation-dissipation theorem (FDT) (Turlier *et al.*, 2016). Here we develop a physical theory for how random motor forces propagate through the complex viscoelastic environment of the cell, which is composed of cytoplasm and cytoskeleton, and the effect of these forces on objects such as ribosomes, mitochondria, and other organelles immersed in the intracellular milieu. We show that depending on the object size, stochastic motor force is not only sufficient to enhance their diffusive transport but can also generate inhomogeneous spatial distributions of these objects, which could provide a mechanism for organelle positioning in cells. The ever present nature of these fluctuating random forces can even enhance molecular motor function itself.

It is well known that biological systems are out of thermal equilibrium. At the length scales of molecular and cellular biology, though, it is much less clear whether these systems are close enough to equilibrium that standard thermodynamics is applicable. A major guiding principle in conceptualizing and modeling processes at these scales has been the FDT, which relates the dissipative part of the linear response of a physical quantity to an external perturbation (e.g., the drag coefficient) to the correlation spectrum of the physical quantity (e.g., the autocorrelation of the velocity), with the relationship depending solely on the temperature (Kubo, 1966;

This article was published online ahead of print in MBoC in Press (http://www.molbiolcell.org/cgi/doi/10.1091/mbc.E19-11-0629) on July 29, 2020.
Author contributions: S.X.S and C.W.W. designed and performed the research, carried out the analysis, and wrote the paper.
*Address correspondence to: Charles W. Wolgemuth (wolg@email.arizona.edu).
Abbreviations used: FDT, fluctuation-dissipation theorem; MSD, mean-squared displacement.

Reichl, 2016). One of the first experiments that suggested a breakdown in the FDT at cellular scales examined oscillations of hair bundles that were perturbed by a small glass fiber and found that a single temperature could not account for the response, nor was the effective temperature equal to the actual temperature of the system (Martin *et al.*, 2001). Later work went on to quantify the magnitude of stochastic motor forces inside cells and showed that the fluctuations of these forces led to enhanced diffusive transport whether or not the particles were large or small compared with the mesh size of the cytoskeleton (Guo *et al.*, 2014).

What are the potential consequences of these nonthermal, motor-driven random forces inside cells? To address this question, we begin by deriving a theory for the dynamics of objects immersed within a cytoplasm driven by random motor forces and random thermal forces. While previous theoretical work has described the characteristics of random motions of the cytoskeleton and cytosol due to motor stochasticity (Lau *et al.*, 2003; Mackintosh and Levine, 2008) and found that in confined actomyosin systems random forces can drive the transport of large organelles, such as the nucleus, to the walls of the confining region (Rupprecht *et al.*, 2018), here we examine motion within the cytoplasm itself and focus on how random forces in the cytoskeleton affect different sized objects. For example, small objects live in the fluid region of the cytoplasm. These objects will not directly experience the shaking of the actin polymers due to molecular motors, but rather feel the jittering motion of the fluid that is induced by the undulating actin and thermal random force. Larger objects, though, are in contact with the actin network and directly experience the jostling of the network. Are these motions equivalent, or are there observable differences between them?

We begin by deriving a theory for the dynamics of objects within the stochastic environment of the cell. We treat the cytoplasm using a two-phase description (Alt and Dembo, 1999; Cogan and Guy, 2010; Li and Sun, 2018), where the cytoskeleton is treated as a viscoelastic network of volume fraction ϕ, surrounded by the viscous cytosol of viscosity η (Figure 1). The motion of the cytoskeleton with respect to the cytosol produces a viscous drag proportional to the difference in velocities. Defining the cytoskeletal and cytosolic velocities as $\mathbf{v}_n$ and $\mathbf{v}_f$, respectively, the force balance on each *phase* (cytoskeleton or cytosol) gives

$$\zeta(\mathbf{v}_n-\mathbf{v}_f)=\nabla\cdot\hat{\sigma}_n+\int\mathbf{H}(\mathbf{x},\mathbf{x}')\cdot\hat{p}_m(\mathbf{x},\mathbf{x}')d^3x'$$

$$\zeta(\mathbf{v}_n-\mathbf{v}_f)=\eta\nabla^2\mathbf{v}_n-\nabla P \tag{1}$$

where P is the hydrostatic pressure and $\hat{\boldsymbol{\sigma}}_n$ is the network stress tensor. In the literature, groups often assume that the actin network is either a viscous fluid or an elastic solid (Mofrad, 2009). To capture both of these behaviors in a single model, we assume that the network stress obeys the Maxwell model:

$$\tau\frac{\partial\hat{\sigma}_n}{\partial t}+\hat{\sigma}_n=\mu\left(\nabla\mathbf{v}_f+(\nabla\mathbf{v}_f)^T\right)+\left(K-\frac{2\mu}{3}\right)(\nabla\cdot\mathbf{v}_f)\hat{\mathcal{I}} \tag{2}$$

with μ and K the shear and bulk viscosities of the network, respectively, and $\hat{\mathcal{I}}$ the identity tensor. Using this assumption (Eq. 2), the cytoskeleton behaves like an elastic solid on times that are shorter than the relaxation time τ and like a viscous fluid on times longer than τ. The model includes the molecular motors using a force density tensor $\hat{p}_m$ that accounts for the average dipole-distributed force **f** exerted by each motor, as well as the average orientation **d** of the motor molecules. If the density of the motor molecules is ρ_m, then

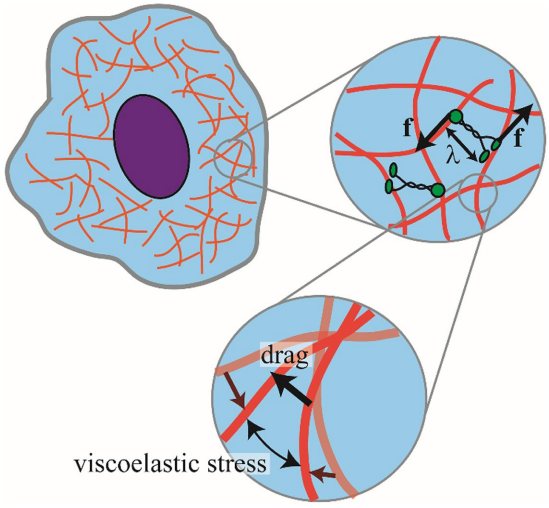

FIGURE 1: The viscoelastic cytoskeleton model. Our two-phase model treats the inside of the cell as a network of cross-linked cytoskeletal filaments (red) immersed in the fluid cytosol (blue). The action of motor molecules (green) exerts equal and opposite forces f on the network at a distance comparable to the size of the motor (λ~100 nm) (Lodish *et al.*, 2000). Movement of the cytoskeleton through the viscous cytosol is resisted by a drag force that is proportional to the difference in velocity between the cytoskeleton and the cytosol. Deformation of the cytoskeletal network produces a viscoelastic stress in the network.

$$\hat{p}_m=\frac{\rho_m\mathbf{fd}}{\lambda} \tag{3}$$

The dipole force is then distributed over the size of the motor molecules, λ, using the kernel

$$\mathbf{H}=\frac{2\pi(\mathbf{x}-\mathbf{x}')}{\lambda^{d+1}}e^{-\frac{\pi(\mathbf{x}-\mathbf{x}')^2}{\lambda^2}} \tag{4}$$

that spreads out the motor force density along the direction of the orientation of the molecule in such a way that the net force is zero, as required by Newton's third law. The force written in this manner acts as a stress on the network, as opposed to treating them as strictly random forces, as in Guo *et al.* (2014). (The network can also experience nonzero random forces that do not obey FDT due to polymerization/depolymerization of the actin. Incorporating these forces into the model follows the same type of procedure and leads to qualitatively similar results.) Under the assumption that the net flow within the cell is zero, the fluid velocity is directly proportional to the cytosolic velocity, $\mathbf{v}_f=-\phi\,\mathbf{v}_n/(1-\phi)$. If we then treat the motor force density as a random matrix, $\hat{p}_m=\hat{\eta}_m$, such that $\langle\hat{\eta}_{m,ij}(\mathbf{x},t)\hat{\eta}_{m,kl}(\mathbf{x}',t')\rangle=c_m^2\delta(\mathbf{x}-\mathbf{x}')\delta(t-t')\delta_{ik}\delta_{jl}$, the cytosolic velocity obeys a damped, stochastic heat equation, which can be solved using a Green's function approach (see the Supplemental Text). The standard deviation (SD) of the motor noise is defined by the parameter c_m.

RESULTS AND DISCUSSION

The motion of objects inside a cell are then driven by two separate stochastic effects, thermal random forces from the environment and stochastic random forces from the molecular motors. We consider two scenarios to determine the motion of these objects. First, for objects that are small compared with the pore size of the actin network (~50–100 nm [Keren *et al.*, 2009; Guo *et al.*, 2014]), the objects interact predominantly with the fluid, and their motion is given by

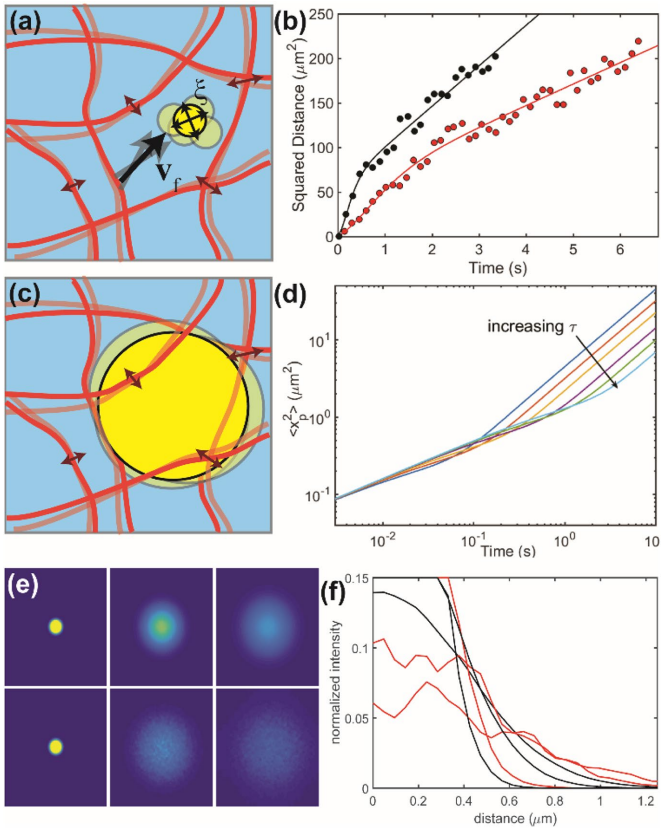

FIGURE 2: The effect of stochastic motor force on objects in the cytoplasm. (a) In the cytoplasm, small objects interact predominantly with the fluid, not the cytoskeleton, and can therefore be modeled as Brownian particles acted on by random thermal forces ξ and adrift within the fluid. The stochastic motor-driven motion of the cytoskeleton (dark red arrows) induces random flows of the fluid (black arrows), and these fluid flows then push on the object. (b) Diffusive spreading of small dye molecules in active cells (black circles) and ATP-depleted cells (red circles) taken from Guo *et al.* (2014) is explained by Eq. 2 (solid lines) with the parameters given in the text. (c) Objects that are larger than the mesh size of the cytoskeleton are restrained by the network and diffuse due to reorganization of the cytoskeleton, which is naturally accounted for by the Maxwell model. For this case, our model leads to slow motion of the particle on short timescales and diffusive behavior for $t < \tau$. (d) Simulations of the stochastic two-phase equations also lead to enhanced diffusion due to motor noise. (e) The color map shows the concentration of diffusing particles that are also advected by the cytosolic velocity induced by motor fluctuations at three different times for cases where the SD of the motor noise was 0.01 (top panel) and 0.1 (bottom panel). (f) Slices through the concentration profile at different times for motor noise SDs of 0.01 (black) and 0.1 (red).

$$\zeta\left(\frac{d\mathbf{x}_p}{dt}-\mathbf{v}_f\right)=\xi_p(t) \tag{5}$$

where $\zeta = 6\pi\eta a$ is the Stokes drag coefficient for a particle of radius a in a fluid of viscosity η, x_p is the position of the object, and ξ_p is the random thermal forces, defined by $\langle\xi_p(t), \xi_p(t')\rangle = 2\zeta k_B T\,\delta(t-t')$ (Figure 2a). To determine the average motion of the object, we want to integrate Eq. 5 to find the mean-squared displacement (MSD). Note that both the random force and the fluid velocity are stochastic variables. As detailed in the Supplemental Text, the solution for the MSD requires some simplifying assumptions. First, we treat the dynamics in one dimension. In addition, we can use relevant time- and length scales to reduce some of the complexity. The timescale over which the network velocity diffuses over a length the size of a molecule is given approximately by $\alpha \sim \eta\lambda^2/G'L^2$, where the viscosity of the cytoplasm is $\eta \sim 10^{-3}$–10^{2} Pa s, the elastic modulus for the cytoskeleton is $G' \sim 1$ Pa (Guo *et al.*, 2014), and $L \sim 100$ nm is the pore size of the actin network (Keren *et al.*, 2009). Therefore, $\alpha \sim 10^{-3}$–10^{-2} s. Microrheology measurements suggest that the relaxation time of the cytoskeleton is $\tau \sim 0.1$–1 s. Therefore, α is reasonably small compared with τ. Using these estimates, we find that the MSD of the object is approximately given by

$$\left\langle x_p(t)^2\right\rangle \sim 2\left(D_p + D_a(\sigma,\phi)\right)t + \Gamma(\sigma,\phi)\left(2\mathrm{erf}\left(\sqrt{t/\tau}\right)-1+\left(\left(\frac{t}{\tau}+1\right)-\frac{2\sqrt{t/\tau}}{\sqrt{\pi}}\left(\frac{t}{\tau}+2\right)\right)e^{-t/\tau}\right) \tag{6}$$

where $D_p \sim 10$ μm²/s is the diffusion coefficient of the object predicted from FDT and the Stokes relation, D_a is a diffusion coefficient due to the stochasticity of the active motors, and Γ is a parameter that also depends on the motor activity. Both D_a and Γ scale as $\sigma\phi^2$, where σ is the variance of the motor fluctuations. We can then define an effective diffusion coefficient, $D_{\mathrm{eff}} = D_a + D_p$. In Guo *et al.* (2014) small dye molecules were observed to diffuse faster in active cells compared with ATP-depleted cells. We find that Eq. 2 is in excellent agreement with measured diffusion data from Figure 7c of Guo *et al.* (2014) of this paper with parameters $D_{\mathrm{eff}} = 22.7$ μm²/s, $\Gamma = 55.2$ μm², and $\tau = 0.12$ s, while for ATP-depleted cells (unfilled points), the best parameters are $D_{\mathrm{eff}} = 12.0$ μm²/s, $\Gamma = 51.0$ μm², and $\tau = 0.42$ s (Figure 2b). Consistent with our model, the data show larger diffusion for active cells than for ATP-depleted cells. Our parameter values for the relaxation times are also consistent with measured values of $\tau \sim 0.1$–1 s (Kole *et al.*, 2005; Hosu *et al.*, 2008; Rubinstein *et al.*, 2009) and suggest that as motor activity is reduced the network may become less dynamic (i.e., with longer relaxation times).

When the object is larger than the size of the meshwork, its motion is strongly hindered by the presence of the actin filaments: To move, the network must reorganize (Figure 2c). Because we directly account for the viscoelasticity of the network through the Maxwell model, our model accounts for dynamic reorientation of the cytoskeleton without additional assumptions. Then, the motion of the particle follows the local motion of the network, $dx_p/dt = v_n$, and we find hindered motion on short timescales and diffusive motion on timescales longer than τ (as shown by the change in slope in Figure 2d that depends on τ). On long timescales, the MSD is (see the Supplemental Text for complete details

$$\left\langle x_p(t)^2\right\rangle \approx \left(\frac{\pi^{\frac{3}{2}}(1-\phi)^2 c_m^2\sqrt{\alpha}}{4\lambda\zeta^2\sqrt{\tau}}\right)t = 2D_{\mathrm{eff}}t \tag{7}$$

This result that the MSD is subdiffusive on short times and then transitions to linear for times greater than τ is qualitatively consistent with previous experiments (Guo *et al.*, 2014). To show that our analytical solutions are consistent with the results from the full two-phase dynamics, we simulated the equations of motion (see Supplemental Text, Eq. 6) and used the resulting velocity to drive an advection-diffusion equation for a concentration. The concentration is found to diffuse more rapidly as the magnitude of the stochastic motor forces increases (Figure 2, e and f).

That random motor forces can lead to enhanced diffusion on long timescales is not surprising. However, we find that motor-driven fluctuations of small objects scale like the square of the volume fraction of the cytoskeleton, whereas the fluctuations of large objects scale like the volume fraction of the cytosol. If we then consider a case where the cytoskeletal density is spatially dependent, then small objects feel increased random forces as they move up the gradient in cytoskeletal density, while large objects will feel increased random forces when they move down a cytoskeletal density gradient. This difference will then result in differential positioning of small and large objects in a cytoskeletal density gradient. To put this on firm theoretical grounds, the Kramers–Moyal expansion provides a way to derive the transport equation for stochastically fluctuating particles (Tabar, 2019). If the random forces are isotropic with an equal probability for moving in the positive and negative directions, then the leading order effect of the fluctuating force is that the particle flux depends on the gradient of the time rate of change of the MSD times the concentration C as

$$J \approx -\nabla\left[\frac{1}{2}\left(\lim_{\tau\to\infty}\left\langle\left(x(t+\tau)-x(t)\right)^2\right\rangle/\tau\right)C\right] \tag{8}$$

This result can be understood physically by considering two containers separated by a small channel. The likelihood that a particle in one container passes through the channel into the other container is related to how large the random fluctuating motions of the particles are. Therefore, if the fluctuations of the particles are larger in one of the containers than in the other, more particles will leave from this container than leave from the other container. That is, there will be a net flux of particles out of the container that has the larger random motions. In the context of objects moving with the cytoskeleton, this suggests that objects smaller than the mesh size will localize in regions of low cytoskeletal density, while objects that are larger than the mesh size will preferentially localize to higher densities of actin. However, it is likely that there will be higher concentrations of motors where the network volume fraction is higher, which would increase the magnitude of the random forces from the motors and could counteract this effect.

As a test of this result, we simulated our two-phase cytoskeleton model with spatially dependent volume fractions of actin, $\phi = \phi_0(1 + 0.8\cos(k_x x)\cos(k_y y))$ (Figure 3). We then solved an advection-diffusion equation for a concentration of particles, with the advection velocity given by either the network velocity (which corresponds to the motion of objects that are large compared with the cytoskeletal velocity) or the cytosolic velocity (for objects smaller than the cytoskeletal velocity). We found that on timescales less than a second, the small objects aggregated in regions of low volume fraction (Figure 3, center panels), while the large objects aggregated in regions of high volume fraction (Figure 3, right panels). The qualitative effect predicted from Eq. 4 is then validated by our numerical simulations of the stochastic two-phase equations, which lead to particle localization consistent with the magnitude of the nonthermal fluctuations.

Another possible consequence of nonthermal cytoskeletal noise is nonuniform spatial positioning of objects in a confined space, such as the cytoplasm of the cell, even when the network volume fraction is uniform. Near confining surfaces, objects experience increased hydrodynamic drag due to wall effects (Happel and Brenner, 1983). However, if the random force obeys FDT, the increased drag is balanced by the random force, and diffusion still drives objects to be uniformly distributed (Dufresne *et al.*, 2000). When FDT breaks down, though, a relationship between the random force and drag is not expected. Consequently, small objects that mostly experience

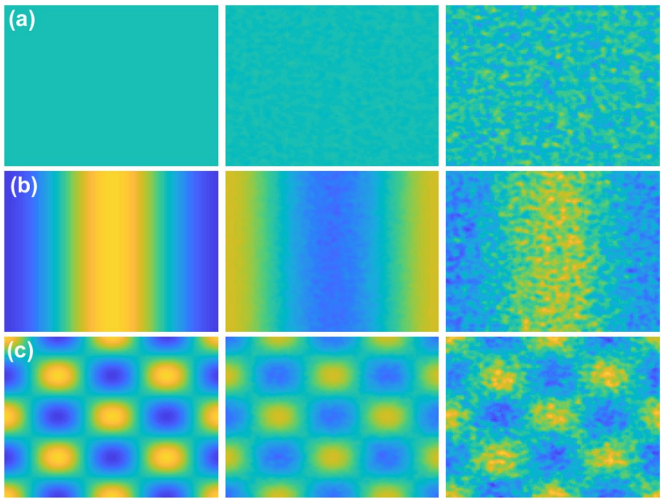

FIGURE 3: Spatial variations in the volume fraction lead to aggregation based on size. Numerical solution of the transport of a concentration of diffusing particles that is also actively driven by random motor forces from the two-phase cytoskeletal model shows aggregation consistent with our predictions. We used a uniform (a) and two spatially dependent concentration profiles (b and c) for the actin cytoskeleton. Time averaging the diffusing particle concentration leads to density profiles that are higher in regions of lower cytoskeletal density for small objects (center panels), whereas large objects aggregate in regions where the cytoskeletal density is highest (right panels). The color map shows low concentrations as blue and high concentrations as yellow. Simulations were performed with the parameters given in the Supplemental Text.

thermal random forcing that obeys FDT will be uniformly distributed in the cell, whereas larger objects, such as mitochondria and even the nucleus, that experience motor-driven random force will be preferentially positioned near surfaces, as predicted previously (Rupprecht *et al.*, 2018). To test whether our model also predicts that large objects preferentially localize in confined regions, we included a finite-sized rigid disk into our fluctuating two-phase cytoskeleton simulations. The rigid disk was implemented using the Moving Boundary Node Method (Wolgemuth and Zajac, 2010), as described in the Supplemental Text. We simulated the motion on an 80×80 grid, corresponding to a 4 μm × 4 μm region; the disk radius was 0.33 μm. We started by simulating the motion of an unconfined object, which was implemented using periodic boundary conditions on the domain. We found that the object's trajectory fluctuated about the starting point (Figure 4a). The MSD for the motion was subdiffusive for short times and then diffusive on long timescales, consistent with the predictions from our analytical results (Figure 2d). We then simulated the disk in a confined region by setting the cytoskeletal velocity to zero on the domain boundaries. We found that the object fluctuated about its starting location, but then executed directed motion toward the bottom wall (Figure 4c). After fluctuating for a period of time near the bottom wall, the object then moved in a directed manner toward the right wall and remained near the bottom right corner of the domain for the remainder of the simulation. The MSD for the confined motion (Figure 4d) showed superdiffusive behavior for short timescales that then slowed at longer timescales. Once the object was at the wall, the MSD was subdiffusive, indicating that it was being attracted toward the walls. These results are similar to those found in Rupprecht *et al.* (2018). Interestingly, though, the Rupprecht *et al.* model involved temporally correlated noise, whereas our model assumes spatially

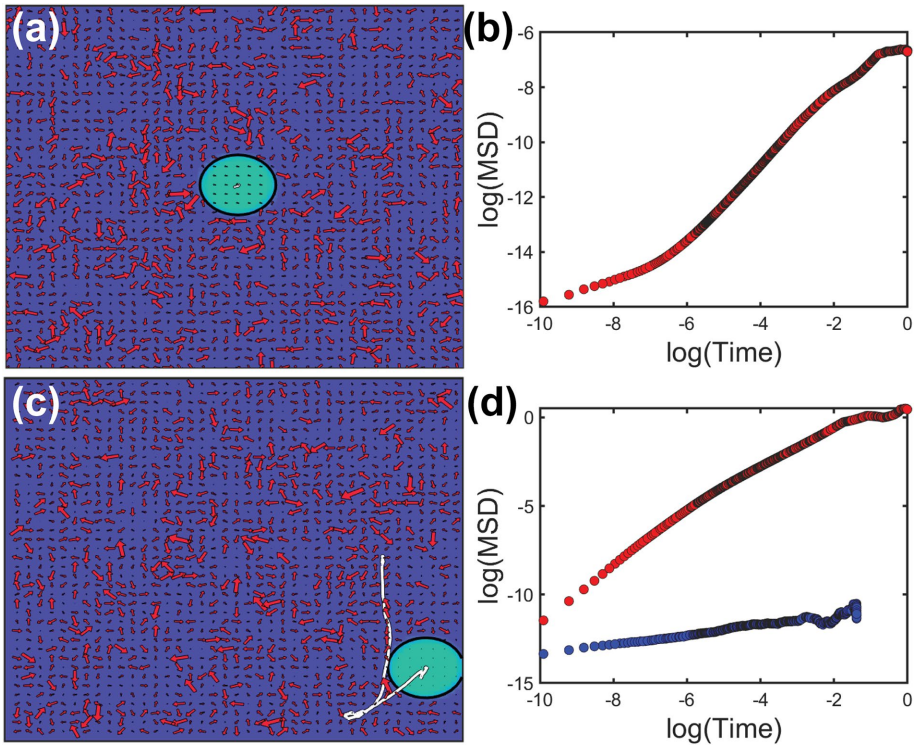

FIGURE 4: Confinement leads to aggregation of large objects near walls. Numerical solution of a finite-sized disk moving in the randomly driven cytoskeleton. (a) Snapshot of the simulation, showing the disk (light blue) and the cytoskeletal velocity vectors (red arrows). There is a white line showing the trajectory of the object (which is barely observable at the center of the object. (b) The MSD of the unconfined object. The MSD is qualitatively similar to what is predicted from our analytical model (Figure 2d). For confined objects (c), the object is attracted toward the walls. The trajectory (white line) is now clearly visible. The object makes large directed motions. (d) The MSD for the particle is qualitatively different from that for the unconfined particle. The full MSD is shown in red. The blue dots show the MSD for the motion during the last 0.2 s of the simulation. This highlights that the object does not move substantially once it gets to the wall

correlated noise. This suggests that nonwhite noise may be sufficient to drive positioning in confined spaces. Since the nucleus in most cells is located near the cell center, these results suggest that nuclear positioning requires active mechanisms to maintain (Almonacid *et al.*, 2015). For mitochondria, active mechanisms are also involved in positioning them near the nucleus in cells such as the oocyte (Duan *et al.*, 2020).

These results suggest other potentially important consequences for organelle positioning in cells (Figure 5, a and b). For example, ribosomes that are comparable in size to the pore size (~20–30 nm) are seen to aggregate near focal adhesions (Willett *et al.*, 2010), where actin is in higher concentrations. In plants, the pollen tube carries male gametes to the female gametophyte (Cai *et al.*, 2014). The structure of a pollen tube is divided into two regions, a nongrowing shank and a domed, apical region, which is where growth occurs. While the tip of the apical region has very little actin, the transition point between the growing region and the shank (sometimes called the "subapex") is filled with an actin-rich structure, known as the fringe. During growth, small secretory vesicles in the pollen tube aggregate at the front of the apical zone, the region mostly devoid of actin, whereas larger vesicles are excluded from this region and remain in the actin-rich shank and subapex (Cai *et al.*, 2014) (Figure 5b). Indeed, actin and myosin are observed to be involved in many aspects of organelle positioning (see Trivedi *et al.*, 2014, and Almonacid *et al.*, 2015, for example), and the results presented here are likely involved. These results also suggest a straightforward experimental test. Cells that are plated on micropatterned patches of extracellular matrix proteins that are asymmetric on lengths smaller than the cell show domains that are enriched in actin (Landere-Grzybowska *et al.*, 2010). Therefore, small dye molecules are predicted to have higher concentrations in regions of lower actin concentration, which can be assessed using confocal microscopy.

Yet another consequence of random motor forces and that different sized particles experience fluctuations that scale differently with cytoskeletal volume fraction is that this leads to the possibility that intracellular processes could use a simple Feynman–Smoluchowski ratchet (Smoluchowski, 1912; Feynman, 1963) to perform meaningful work (Figure 5c). For example, molecular motors, like myosin, are smaller than the actin mesh size, whereas the cargo they transport is much larger. Therefore, a single myosin molecule (which acts like the ratchet and the pawl) experiences nonthermal random forces from the sloshing of the cytosol (proportional to ϕ), whereas the cargo feels the nonthermal random forces of the shaking of the cytoskeleton ($\propto(1-\phi)$). Since the magnitude of the force fluctuations is somewhat analogous to the temperature, then motor molecules (the ratchet), such as kinesin, myosin, and dynein, which are smaller than the mesh size, will experience fluctuations (an effective temperature) that are smaller than that of the cargo (the paddle). In this case, we expect that the motor molecule will move faster than it would in the presence of purely thermal fluctuations.

Here we have shown that the stochasticity of intracellular motors can lead to a number of unexpected consequences, such as enhanced diffusion of small objects, object sorting based on size (which provides a mechanism for organelle positioning), and size-dependent fluctuations that can enable Feynman–Smoluchowski ratchets to do useful work. The principal components of our model that lead to the behavior that we describe are 1) a porous cytoskeletal network immersed in a viscous cytosol, 2) molecular motors that exert random forces on the network, and 3) dynamic reorganization of the elastic components of the network. Therefore, other rheological descriptions of the cytoskeleton that still contain these three components, such as soft glassy rheology (Madadapu *et al.*, 2008), should lead to behavior similar to what is described here. We point out that the last of these requirements is important because, for a purely elastic solid network, objects that are larger than the pore size are expected to be stuck to the network. If the network does not reorganize, the object cannot free itself from its local bonds and it will not diffuse. The experiments we suggest here can be performed to validate our work and to determine the magnitude of these effects within cells. Taken as a whole, these results constitute an understanding of how cells can use motor stochasticity to drive intracellular processes.

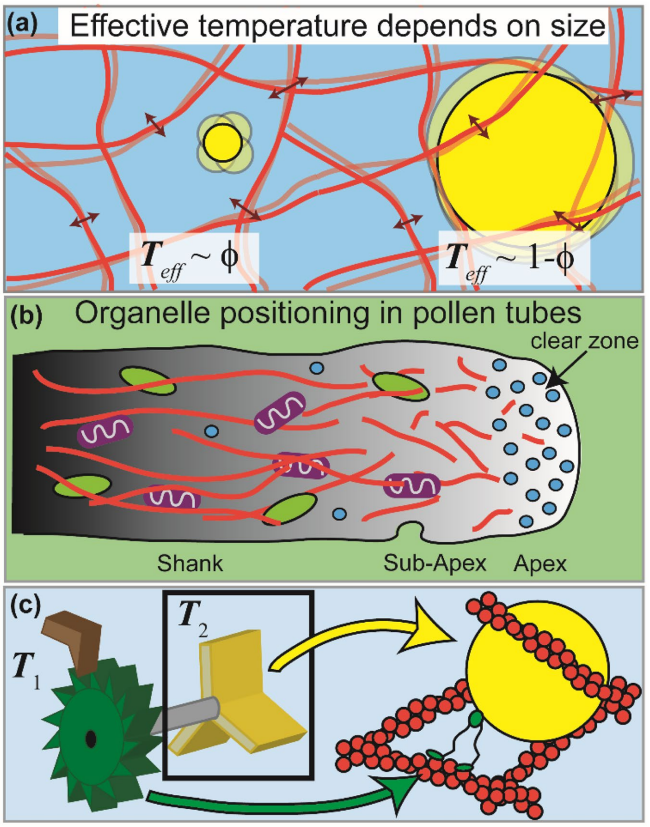

FIGURE 5: Size dependence of the effective temperature can drive cellular functions. (a) Our model predicts that small objects experience an effective temperature proportional to the cytoskeletal volume fraction ϕ, whereas objects that are larger than the mesh size experience an effective temperature proportional to $1 - \phi$. One consequence of this effect is that smaller objects can get repelled from regions of high volume fraction, while larger objects will be attracted to these regions. For example, in pollen tubes (b), small vesicles are localized near the tip (the apex), which is largely devoid of actin (red filaments) (Cai *et al.*, 2014). The shank and subapex have more actin, and larger organelles are localized in these regions. (c) A size-dependent effective temperature can also lead to an operational Feynman–Smoluchowski ratchet, which may impact molecular motors. If the ratchet (green) and pawl (brown) are at a lower temperature than the paddle (yellow), then the ratchet can do work. In cells, the ratchet and pawl are analogous to a molecular motor, such as myosin (green), and the paddle is analogous to the cargo (yellow).

ACKNOWLEDGMENTS

This research was supported by National Institute of Health Grant U54CA210172.

REFERENCES

Almonacid M, Ahmed WW, Bussonnier M, Mailly P, Betz T, Voituriez R, Gov NS, Verlhac M-H (2015). Active diffusion positions the nucleus in mouse oocytes. Nat Cell Biol 17, 470–479.

Alt W, Dembo M (1999). Cytoplasm dynamics and cell motion: two-phase flow models. Math Biosci 156, 207–228.

Cai G, Parrotta L, Cresti M (2014). Organelle trafficking, the cytoskeleton, and pollen tube growth. J Int Plant Biol 57, 63–78.

Cogan NG, Guy RD (2010). Multiphase flow models of biogels from crawling cells to bacterial biofilms. HFSP J 4, 11–25.

Duan X, Li Y, Yi K, Guo G, Wang H, Wu PH, Yang J, Mair D, Obregon EM, Kalab P, *et al.* (2020). Organelle distribution initiates actin-based spindle migration in mouse oocytes. Nat Commun 11, 227.

Dufresne ER, Squires TM, Brenner MP, Grier DG (2000). Hydrodynamic coupling of two Brownian spheres to a planar surface. Phys Rev Lett 85, 3317–3320.

Feynman RP (1963). The Feynman Lectures on Physics, Vol. 1, Boston, MA: Addison-Wesley.

Guo M, Ehrlicher AJ, Jensen M-H, Renz M, Moore JR, Goldman RD, Lippincott-Schwartz J, Mackintosh FC, Weitz DA (2014). Probing the stochastic, motor-driven properties of the cytoplasm using force spectrum microscopy. Cell 158, 822–832.

Happel J, Brenner H (1983). Low Reynolds Number Hydrodynamics, Dordrecht, Netherlands: Springer Netherlands.

Hosu BG, Mullen SF, Critser JK, Forgacs G (2008). Reversible disassembly of the actin cytoskeleton improves the survival rate and developmental competence of cryopreserved mouse oocytes. PLoS One 3, e2787.

Keren K, Yam PT, Kinkhabwala A, Mogilner A, Theriot JA (2009). Intracellular fluid flow in rapidly moving cells. Nat Cell Biol 11, 1219–1224.

Kole TP, Tseng Y, Jiang I, Katz JL, Wirtz D (2005). Intracellular mechanics of migrating fibroblasts. Mol Biol Cell 16, 328–338.

Kolomeisky AB, Fisher ME (2007). Molecular motors: a theorist's perspective. Annu Rev Phys Chem 58, 675–695.

Kubo R (1966). The fluctuation-dissipation theorem. Rep Prog Phys 29, 255–284.

Landere-Grzybowska K, Soh S, Mahmud G, Komarova Y, Pilans D, Grzybowski BA (2010). Short-term molecular polarization of cells on symmetric and asymmetric micropatterns. Soft Matter 6, 3257–3268.

Lau AWC, Hoffman BD, Davies A, Crocker JC, Lubensky TC (2003). Microrheology, stress fluctuations, and active behavior of living cells. Phys Rev Lett 91, 198101.

Li Y, Sun SX (2018). Transition from actin-driven to water-driven cell migration depends on external hydraulic resistance. Biophys J 114, 2965–2973.

Lodish H, Berk A, Zipursky SL, Matsudaira P, Baltimore D, Darnell J (2000). Molecular Cell Biology, 4th Ed., New York: W.H. Freeman.

Mackintosh FC, Levine AJ (2008). Nonequilibrium mechanics and dynamics of motor-activated gels. Phys Rev Lett 100, 018104.

Madadapu KK, Govindjee S, Mofrad MR (2008). On the cytoskeleton and soft glassy rheology. J Biomech 41, 1467–1478.

Martin P, Hudspeth AJ, Julicher F (2001). Comparison of a hair bundle's spontaneous oscillations with its response to mechanical stimulation reveals the underlying active process. Proc Natl Acad Sci USA 98, 14380–14385.

Mofrad MRK (2009). Rheology of the cytoskeleton. Annu Rev Fluid Mech 41, 433–453.

Oster G (2002). Brownian ratchets: Darwin's motors. Nature 417, 25.

Reichl LE (2016). A Modern Course in Statistical Physics, 4th Ed., Berlin: Wiley-VCH.

Rubinstein B, Fournier MF, Jacobson K, Verkhovsky AB, Mogilner A (2009). Actin-myosin viscoelastic flow in the keratocyte lamellipod. Biophys J 97, 1853–1863.

Rupprecht J-F, Vishen AS, Shivashankar GV, Rao M, Prost J (2018). Maximal fluctuations of confined actomyosin gels: dynamics of the cell nucleus. Phys Rev Lett 120, 098001.

Smoluchowski MV. (1912). Experimentell nachweisbare, der Ublichen Thermodynamik widersprechende Molekularphenomene. Phys Zeitschur 13, 1069.

Tabar MRR (2019). Kramers-Moyal expansion and Fokker-Planck equation. In: Analysis and Data-Based Reconstruction of Complex Nonlinear Dynamical Systems, Cham, Switzerland: Springer Nature.

Trivedi N, Ramahi JS, Karakaya M, Howell D, Kerekes RA, Solecki DJ (2014). Leading-process actomyosin coordinates organelle positioning and adhesion receptor dynamics in radially migrating cerebellar granule neurons. Neural Devel 9, 26.

Turlier H, Fedosov DA, Audoly B, Auth T, Gov NS, Sykes C, Joanny J-F, Compper G, Betz T (2016). Equilibrium physics breakdown reveals the active nature of red blood cell flickering. Nat Phys 12, 513–519.

Willett M, Pollard HJ, Vlasak M, Morley SJ (2010). Localization of ribosomes and translation initiation factors to talin/beta3-integrin-enriched adhesion complexes in spreading and migrating mammalian cells. Biol Cell 102, 265–276.

Wolgemuth CW, Zajac M (2010). The Moving Boundary Node Method: a level set-based, finite volume algorithm with applications to cell motility. J Comput Phys 229, 7287–7308.